 doi:10.20944/preprints202203.0098.v1

*Article*

# Dynamic model and response analysis of gear-rotor-bearing systems with bearing fitting clearances

**Fengtao Wang [1], Peng Dai [1,*], Jianping Wang [1], Linkai Niu [2]**

[1] Anhui Polytechnic University, Wuhu, 241000, China; tjqhd@163.com
[2] Taiyuan University of Technology, Taiyuan 030024, China; niulinkai@tyut.edu.cn
* Correspondence: daipeng_ahpu@163.com (P. D.); wangfengt@1985@163.com (F. W.)

**Abstract:** Mechanical power and motion are often transmitted by the gear-rotor-bearing system. When there are fitting clearances between the housing and outer ring in bearings, complex vibration responses will be generated, which makes the operating status difficult to identify. Therefore, for analyzing dynamic responses, a dynamic model of gear-rotor-bearing systems with bearing fitting clearances is proposed. In the model, the bearing system with fitting clearances and gear pair system are combined, and the coupling relationship is determined by the gyroscopic motion of the shaft. The friction force and collision force caused by fitting clearances are also considered, which are simulated by the Coulomb friction model and Hertz theory. The result shows that the meshing stiffness will also be excited by the bearing displacement. When there are fitting clearances on the bearing, the amplitude modulation of the bearing outer raceway to the system time-domain response is intensified, and the multiple harmonic frequency of bearings and gear pairs are generated on the spectrum, as well as defect frequencies of gear pairs. As the fitting clearance is increased, the higher multiple harmonic responses will be caused. Although the response amplitude of the gearbox is increased by raising the input speed, multiple harmonic responses are suppressed, which makes the system mainly vibrate at the fundamental frequency. Then, the dynamic model and the vibration analysis are experimentally verified.

**Keywords:** Gear-rotor-bearing system; bearing fitting clearance; vibration response; rotating speed; multiple harmonic response

## 1. Introduction

The gear-rotor-bearing system is usually used to transmit mechanical power and motion in the modern machinery industry, in which the bearing plays the role of providing the necessary support for the rotating shaft, and the speed, torque and rotation direction are regulated by the gear pair [1, 2]. However, the fitting clearance between the housing and outer ring in bearings is easily caused by unfavorable factors such as manufacturing, assembly, fatigue, wear, and temperature [3, 4]. For bearings that rotate at high speeds, collisions and friction between the connecting surfaces are generated due to the fitting clearance, which may cause severe looseness, imbalance, misalignment and other failures [5,6]. Moreover, the vibration of the bearing with fitting clearances is propagated to the gear pair by the rotor, the abnormal meshing of the gear pair is caused, and the degree of system failure may be deepened [7], and the performance and service life will be greatly reduced [8,9]. In addition, the complexity of the vibration response generated by the transmission system is greatly increased, which makes the identification of operating conditions more difficult. Thus, it is significant to realize the response analysis of gear-rotor-bearing systems with bearing fitting clearances by establishing a dynamic model.

The response characteristic of the system is seriously affected by the operating state of support bearings, and the dynamic response of bearings with fitting clearances has been

 doi:10.20944/preprints202203.0098.v1

studied by many researchers. The effect of fitting clearances on vibration responses of bearings was studied by Gustafsson, and the results showed that the amplitude of bearing vibration was increased by the increased clearance [10]. Through the established dynamic model, the meshing stiffness and load distribution of gear pairs in the planetary gear train with bearing fitting clearances was studied by Kahraman [11, 12]. Based on this model, the tooth wedging in a planetary gearbox considering bearing fitting clearances was analyzed by GUO [13]. A mathematical model of the planetary gear train was proposed by Chen for vibration analysis [14], in which the bearing fitting clearances and sun gear crack defects were considered. The model for simulating the rolling bearing fitting clearance and load was established by TomovićR [15], and the effect of fitting clearances on the load distribution was further discussed through this model. When a model of bearings with the radial clearance between stationary parts and rotating parts was proposed by Mizuho Inagaki et al. [16], the non-linear resonance and self-excited vibration were found, then the generation mechanism of self-excited vibration were revealed. The different support forms of the ball bearing balanced rigid rotor were simulated by M. Tiwari [17], and the effect of radial clearances on the vibration response of the rotor was also studied.

When there are fitting clearances between the housing and out ring in bearings, other problems may be brought up, such as loosening of the connecting component and nonlinear vibration. In the past few years, these problems have gradually got the attention of many researchers. When the dynamic response of bearings with support looseness was studied by Chu [18], the nonlinear damping and stiffness were considered, and the shooting method and Floquet theory were used for the periodic solution, then the stability of solutions was further discussed. The model of bearing-rotor systems with loose failure was established by M. Behzad using the energy method [19]. Through this dynamic model, the loose disc was found to perform gyroscopic motion, and the vibration response of rotors can be expressed as a function of the clearance between the loosening disc and the shaft. The loosening failure of the rotor system was studied by Lu through experiments [20], the bearing looseness was simulated through the pre-tightened bolts of the bearing housing, and the nonlinear response was analyzed through the frequency spectrum and the axis track. It was found that the fractional harmonic responses and multiple harmonic responses of the rotor were generated when there were loosening failures on the rotor system.

The evaluation of the health status is based on the response analysis of the gearbox, and the response characteristics of the bearing and gear pair are widely studied through experiments, established models and finite element methods [21]. The vibration responses of gear pairs with the crack defect were explained by Ian Howard et al. using the established dynamic model [22], and the meshing stiffness was simulated by the finite element method. A dynamic model with 6 DOFs of gear pairs was established by Parey et al. [23], and the conclusions obtained can be referenced for the fault diagnosis of gearboxes. Based on this dynamic model, Wan improved the method for calculating meshing stiffness [24], which was verified by experiments and finite element methods, and the response analysis of gear pairs was realized. The energy method was used by Ma for the dynamic excitation of gear pairs with crack defects and spalling defects [25], the changes in the dynamic excitation and vibration characteristics of gear pairs were revealed in detail. This method was followed by a large number of researchers and frequently used in subsequent vibration analysis of gear pairs. As for the existing research on response characteristics of ball bearings, the localized failure of bearings was described by the impulse function, and the model of the bearing with localized failures was extended to compound failures, then the dynamic response of bearings with multi-point defects was studied by McFadden and Smith [26, 27]. For understanding the influence of load and shock waveforms on the response of bearings, Choudhury and Tandon [28] built a dynamic model for describing the localized defect in ball bearings. The constant-period sequence was replaced by tiny random variables, and the improvement of the analytical model was realized by Ho [29]. The

 doi:10.20944/preprints202203.0098.v1

contact between the roller and raceway was simplified to a spring-damper by Patil et al. [30], and a new dynamic model of bearings was bulit based on the Hertz contact theory. Sawalhi proposed a comprehensive model of gear-shaft-bearing systems, and the compound defects in bearings and gear pairs were considered, finally the correctness of this dynamic model was verified by theory and experiments.

In summary, the vibration responses of gearboxes have been explained by many researchers through established models. However, the established model is mainly for the bearing system or gear pair system, the cooperative operation of gears and bearings is ignored, and the gear-rotor-bearing system is rarely considered comprehensively. In existing dynamic models of gear-shaft-bearing systems, gear pairs and bearings are normally set to work independently, and the coupling relationship between the two is weakened, so that the vibration response obtained by the model is far from the vibration response obtained by the experiment. Moreover, when there are fitting clearances between the housing and outer ring in bearings, the dynamic characteristic of gearboxes is seriously affected by the abnormality of the supporting parts, which brings great difficulty to the identification of the operating status. Thus, a dynamic model of the gear-rotor-bearing system with bearing fitting clearances is established for the vibration analysis. In this model, the bearing system with fitting clearances and the gear pair system are combined, and the coupling relationship between the two is determined by the gyroscopic motion of the shaft, then the dynamic response of the gear-rotor-bearing system with bearing fitting clearances are analyzed. At last, the dynamic model and the vibration analysis are experimentally verified.

## 2. Dynamic model of gear-rotor-bearing systems with bearing fitting clearances

### *2.1 Model assumptions*

Since the vibration generation of gear-rotor-bearing systems is extremely intricate, it is necessary to make reasonable simplifications and basic assumptions when establishing the model, and in these assumptions only the main factors that affect the vibration response are considered. The concrete assumptions made are as follows:

(1) When there are fitting clearances between the housing and outer ring in bearings, the outer ring can be displaced in the radial direction, and the rotational angular displacement is not considered. The housing is fixed and the response of the bearing resonator can be extracted for vibration analysis.

(2) The motion between the ball and raceway is assumed to be pure rolling, and the elastic deformation of the bearing satisfies the Hertzian contact theory.

(3) The bending deformation of the shaft is ignored during the transmission process.

(4) The axial displacement of bearings and gear pairs is not considered.

(5) The gyroscopic movement of the low-speed shaft is ignored, and the gyroscopic movement of the high-speed shaft is the main cause of offset angle and center distance error.

### *2.1 Dynamic model of gear-rotor-bearing systems*

As shown in Figure 1, a dynamic model of gear-rotor-bearing systems with 36 DOFs is built according to the Lagrange equation. And the dynamic equations are given as follows [31]:

Preprints (www.preprints.org) | NOT PEER-REVIEWED | Posted: 7 March 2022 doi:10.20944/preprints202203.0098.v1

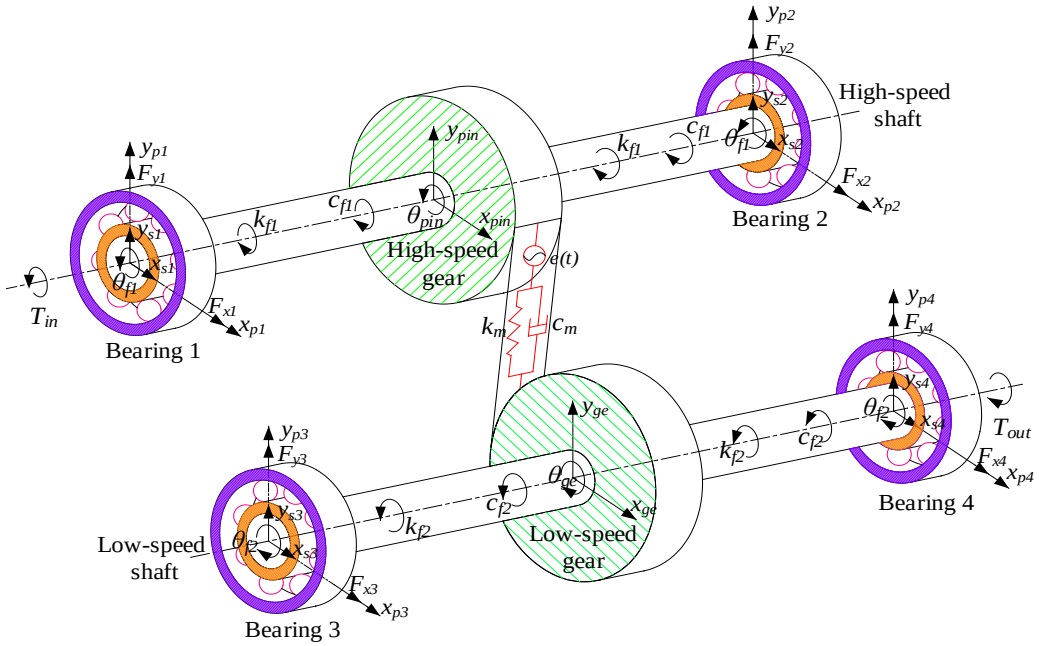


**Figure 1.** Model of gear-rotor-bearing systems.

The motion control equation of the high-speed shaft is:

$$I_{f1}\ddot{\theta}_{f1} + c_{f1}(\dot{\theta}_{f1} - \dot{\theta}_{pin}) + k_{f1}(\theta_{f1} - \theta_{pin}) = T_{in} \tag{1}$$

The motion control equations of the bearing 1 are:

$$\begin{cases} m_{s1}\ddot{x}_{s1} + c_{sx1}(\dot{x}_{s1} - \dot{x}_{pin}) + k_{sx1}(x_{s1} - x_{pin}) + f_{x1} = 0 \\ m_{s1}\ddot{y}_{s1} + c_{sy1}(\dot{y}_{s1} - \dot{y}_{pin}) + k_{sy1}(y_{s1} - y_{pin}) + f_{y1} = 0 \\ m_{p1}\ddot{x}_{p1} + c_{px1}\dot{x}_{p1} + k_{px1}x_{p1} - f_{x1} = F_x \\ m_{p1}\ddot{y}_{py1} + (c_{py1} + c_{r1})\dot{y}_{p1} + (k_{py1} + k_{r1})y_{p1} - k_{r1}y_{r1} - c_{r1}\dot{y}_{r1} - f_{y1} = F_y \\ m_{r1}\ddot{y}_{r1} + c_{r1}(\dot{y}_{r1} - \dot{y}_{p1}) + k_{r1}(y_{r1} - y_{p1}) = 0 \end{cases} \tag{2}$$

The motion control equations of the high-speed gear are:

$$\begin{cases} I_{pin}\ddot{\theta}_{pin} - c_{f1}(\dot{\theta}_{f1} - \dot{\theta}_{pin}) - k_{f1}(\theta_{f1} - \theta_{pin}) = -R_{pin}F_M \\ m_{pin}\ddot{x}_{pin} + c_{sx1}(\dot{x}_{pin} - \dot{x}_{s1}) + c_{sx2}(\dot{x}_{pin} - \dot{x}_{s2}) + k_{sx1}(x_{pin} - x_{s1}) + k_{sx2}(x_{pin} - x_{s2}) = 0 \\ m_{pin}\ddot{y}_{pin} + c_{sy1}(\dot{y}_{pin} - \dot{y}_{s1}) + c_{sy2}(\dot{y}_{pin} - \dot{y}_{s2}) + k_{sy1}(y_{pin} - y_{s1}) + k_{sy2}(y_{pin} - y_{s2}) = F_M \end{cases} \tag{3}$$

The motion control equations of the bearing 2 are:

$$\begin{cases} m_{s2}\ddot{x}_{s2} + c_{sx2}(\dot{x}_{s2} - \dot{x}_{pin}) + k_{sx2}(x_{s2} - x_{pin}) + f_{x2} = 0 \\ m_{s2}\ddot{y}_{s2} + c_{sy2}(\dot{y}_{s2} - \dot{y}_{pin}) + k_{sy2}(y_{s2} - y_{pin}) + f_{y2} = 0 \\ m_{p2}\ddot{x}_{p2} + c_{px2}\dot{x}_{p2} + k_{px2}x_{p2} - f_{x2} = 0 \\ m_{p2}\ddot{y}_{py2} + (c_{py2} + c_{r2})\dot{y}_{p2} + (k_{py2} + k_{r2})y_{p2} - k_{r2}y_{r2} - c_{r2}\dot{y}_{r2} - f_{y2} = 0 \\ m_{r2}\ddot{y}_{r2} + c_{r2}(\dot{y}_{r2} - \dot{y}_{p2}) + k_{r2}(y_{r2} - y_{p2}) = 0 \end{cases} \tag{4}$$

The motion control equations of the bearing 3 are:

$$\begin{cases} m_{s3}\ddot{x}_{s3} + c_{sx3}(\dot{x}_{s3} - \dot{x}_{ge}) + k_{sx3}(x_{s3} - x_{ge}) + f_{x3} = 0 \\ m_{s3}\ddot{y}_{s3} + c_{sy3}(\dot{y}_{s3} - \dot{y}_{ge}) + k_{sy3}(y_{s3} - y_{ge}) + f_{y3} = 0 \\ m_{p3}\ddot{x}_{p3} + c_{px3}\dot{x}_{p3} + k_{px3}x_{p3} - f_{x3} = 0 \\ m_{p3}\ddot{y}_{p3} + (c_{py3} + c_{r3})\dot{y}_{p3} + (k_{sp3}+k_{r3})y_{p3} - k_{r3}y_{r3} - c_{r3}\dot{y}_{r3} - f_{y3} = 0 \\ m_{r3}\ddot{y}_{r3} + c_{r3}(\dot{y}_{r3} - \dot{y}_{p3}) + k_{r3}(y_{r3} - y_{p3}) = 0 \end{cases} \tag{5}$$

The motion control equations of the low-speed gear are:

Preprints (www.preprints.org) | NOT PEER-REVIEWED | Posted: 7 March 2022 doi:10.20944/preprints202203.0098.v1

$$\begin{cases} I_{ge}\ddot{\theta}_{ge} - c_{f2}(\dot{\theta}_{f2} - \dot{\theta}_{ge}) - k_{f2}(\theta_{f2} - \theta_{ge}) = R_{ge}F_M \\ m_{ge}\ddot{x}_{ge} + c_{sx3}(\dot{x}_{ge} - \dot{x}_{s3}) + c_{sx4}(\dot{x}_{ge} - \dot{x}_{s4}) + k_{sx3}(x_{ge} - x_{s3}) + k_{sx4}(x_{ge} - x_{s2}) = 0 \\ m_{ge}\ddot{y}_{ge} + c_{sy3}(\dot{y}_{ge} - \dot{y}_{s3}) + c_{sy4}(\dot{y}_{ge} - \dot{y}_{s4}) + k_{sy3}(y_{ge} - y_{s3}) + k_{sy4}(y_{ge} - y_{s4}) = 0 \end{cases} \quad (6)$$

The motion control equations of the bearing 4 are:

$$\begin{cases} m_{s4}\ddot{x}_{s4} + c_{sx4}(\dot{x}_{s4} - \dot{x}_{ge}) + k_{sx4}(x_{s4} - x_{ge}) + f_{x4} = 0 \\ m_{s4}\ddot{y}_{s4} + c_{sy4}(\dot{y}_{s4} - \dot{y}_{ge}) + k_{sy4}(y_{s4} - y_{ge}) + f_{y4} = 0 \\ m_{p4}\ddot{y}_{p4} + (c_{px4} + c_{r4})\dot{y}_{p4} + (k_{px4} + k_{r4})y_{p4} - k_{r4}y_{r4} - c_{r4}\dot{y}_{r4} - f_{y4} = 0 \\ m_{r4}\ddot{y}_{r4} + c_{r4}(\dot{y}_{r4} - \dot{y}_{p4}) + k_{r4}(y_{r4} - y_{p4}) = 0 \end{cases} \quad (7)$$

The motion control equation of the low-speed shaft is:

$$I_{f2}\ddot{\theta}_{f2} + c_{f2}(\dot{\theta}_{f2} - \dot{\theta}_{ge}) + k_{f2}(\theta_{f2} - \theta_{ge}) = -T_{out} \quad (8)$$

Where, $I_{f1}, I_{f2}, I_{pin}$ and $I_{ge}$ represent the moment of inertia of the high-speed shaft, low-speed shaft, high-speed gear and low-speed gear; $\theta_{f1}, \theta_{f2}, \theta_{pin}$ and $\theta_{ge}$ represent the moment of inertia of the high-speed shaft, low-speed shaft, high-speed gear and low-speed gear; $m_{pin}, m_{ge}, m_{pj}, m_{sj}$ and $m_{rj}$ $(j = 1,2 \dots)$ are the mass of the high-speed gear, low-speed gear, bearing outer ring, bearing inner ring and bearing resonator; $k_{sxj}$ and $k_{syj}$ $(j = 1,2 \dots)$ are the supporting stiffness of the bearing inner ring; $c_{sxj}$ and $c_{syj}$ $(j = 1,2 \dots)$ are the supporting damping of the inner ring; $k_{pxj}$ and $k_{pyj}$ $(j = 1,2 \dots)$ are the supporting stiffness of the bearing outer ring; $c_{pxj}$ and $c_{pyj}$ $(j = 1,2 \dots)$ are the supporting damping of the outer ring; $k_{ryj}$ and $c_{ryj}$ $(j = 1,2 \dots)$ are the supporting stiffness and supporting damping of the bearing resonator; $x_{pin}, x_{ge}, x_{pj}$ and $x_{sj}$ $(j = 1,2 \dots)$ are the linear displacement of the high-speed gear, low-speed gear, bearing outer ring and inner ring in the x direction; $y_{pin}, y_{ge}, y_{pj}, y_{sj}$ and $y_{rj}$ $(j = 1,2 \dots)$ are the linear displacement in the y direction; $T_{in}$ and $T_{out}$ are the input torque and output torque; $R_{pin}$ and $R_{ge}$ represent the base circle radius of the high-speed gear and low-speed gear.

In the bearing system, the contact force between balls and raceways in the x-direction and y-direction are represented by $f_{xj}$ and $f_{yj}$ $(j = 1,2 \dots)$. The bearing 1 is used as an example, based on the Hertzian theory, the contact force can be simulated as:

$$\begin{cases} f_{x1} = k_{re1}\sum_{i=1}^{n_b}(\gamma_i \varepsilon_i^n \cos\theta_i) \\ f_{y1} = k_{re1}\sum_{i=1}^{n_b}(\gamma_i \varepsilon_i^n \sin\theta_i) \end{cases} \quad (9)$$

Where: $k_{re1}$ represents the equivalent stiffness between the bearing raceway and balls; $n_b$ is the total number of the bearing ball; $i$ is the serial number of balls; $n$ is 1.5 for the ball bearings; Whether the ball is in contact with the raceway is judged by $\gamma_i$, and its expression is:

$$\gamma_i = \begin{cases} 1 & \delta_i > 0 \\ 0 & \text{else} \end{cases} \quad (10)$$

$\theta_i$ represents the circumferential position of bearing balls, which is determined by *Eq* (11):

$$\theta_i = \frac{2\pi(i-1)}{n_b} + \left(1 - \frac{d_b}{d_m}\right)\frac{w_s}{2}t + \theta_0 \quad (11)$$

Where, $d_m$ is the diameter of the pitch circle; $d_b$ represents the diameter of balls; $w_s$ represents the rotating speed; $\theta_0$ represents the phase of bearing cages.

Preprints (www.preprints.org) | NOT PEER-REVIEWED | Posted: 7 March 2022 doi:10.20944/preprints202203.0098.v1

$\varepsilon_i$ represents the contact deformation between balls and raceways, which can be calculated as:

$$\varepsilon_i = (x_s - x_p)\cos\theta_i + (y_s - y_p)\sin\theta_i - c_o \tag{12}$$

Where, $c_o$ represents the bearing clearance.

$$\begin{cases} F_M = F_k + F_c \\ F_k = k_t\left(R_{pin}\theta_{pin} - R_{ge}\theta_{ge} - y_{pin} + y_{ge} - \widetilde{e_t}\right) \\ F_c = c_t\left(R_{pin}\dot{\theta}_{pin} - R_{ge}\dot{\theta}_{ge} - \dot{y}_{pin} + \dot{y}_{ge} - \dot{\widetilde{e}_t}\right) \end{cases} \tag{13}$$

Where, $F_M$ represents the meshing force of gear pairs [33], which can be divided into elastic force $F_k$ and viscous force $F_c$; $c_t$ and $k_t$ are meshing damping and meshing stiffness of gear pairs.

$$\frac{1}{k_t} = \begin{cases} \sum_{i=1}^{2}\left(\frac{1}{k_{b1,i}} + \frac{1}{k_{s1,i}} + \frac{1}{k_{a1,i}} + \frac{1}{k_{h,i}} + \frac{1}{k_{f1,i}} + \frac{1}{k_{s2,i}} + \frac{1}{k_{f2,i}} + \frac{1}{k_{a2,i}} + \frac{1}{k_{\tau1,i}} + \frac{1}{k_{b2,i}} + \frac{1}{k_{\tau2,i}}\right) & \text{double tooth} \\ \frac{1}{k_{b1}} + \frac{1}{k_{s1}} + \frac{1}{k_{a1}} + \frac{1}{k_h} + \frac{1}{k_{f1}} + \frac{1}{k_{b2}} + \frac{1}{k_{s2}} + \frac{1}{k_{a2}} + \frac{1}{k_h} + \frac{1}{k_{f2}} + \frac{1}{k_{\tau1}} + \frac{1}{k_{\tau2}} & \text{single tooth} \end{cases} \tag{14}$$

$\widetilde{e_t}$ represents the transmission fluctuation and is simulated by the trigonometric functions in this paper [34].

$$\widetilde{e_t} = e_o + e_m\sin(2\pi f_m t + \varphi) \tag{15}$$

Where, $e_o$ and $e_m$ are the average transmission fluctuation and fluctuation range; $f_m$ is the fundamental frequency of meshing frequencies.

### *2.3 Gyroscopic motion of the high-speed shaft*

The gyroscopic movement of the shaft is caused by asynchronous vibration of bearing inner rings at both sides, then bearing systems and gear systems can be connected using this way. Also, the offset angle and center distance error caused by the gyroscopic motion can be used to determine the vibration transmission between bearings and gear pairs. As shown in Figure 2, the modulus of the $\overrightarrow{BE_0}$ is the actual center distance $a$ of gear pairs, and the angle between $\overrightarrow{AC}$ and $\overrightarrow{D_0F_0}$ is the offset angle $\theta$ of the two shafts. The following equations is given.

$$\theta = \arccos\frac{\sqrt{(x_{s2} - x_{s1})^2 + (y_{s2} - y_{s1})^2}}{\sqrt{(x_{s2} - x_{s1})^2 + (y_{s2} - y_{s1})^2 + L^2}} \tag{16}$$

$$a = \sqrt{\left[a_0 - \frac{1}{2}(x_{s1} + x_{s2})\right]^2 + \frac{1}{4}(y_{s1} + y_{s2})^2} \tag{17}$$

Where, $L$ represents the length of shafts.

### *2.4 Meshing stiffness of gear pairs*

When the actual center distance and offset angle caused by gyroscopic movement of shafts are considered, the model for calculating meshing stiffness can be established according to the potential energy method. [35]. In particular, when the two shafts are not parallel, the direction of the force between the meshing teeth will be changed, as shown in Figure 3, and the beam model for calculating the dynamic excitation is given in Figure 4.

Preprints (www.preprints.org) | NOT PEER-REVIEWED | Posted: 7 March 2022 doi:10.20944/preprints202203.0098.v1

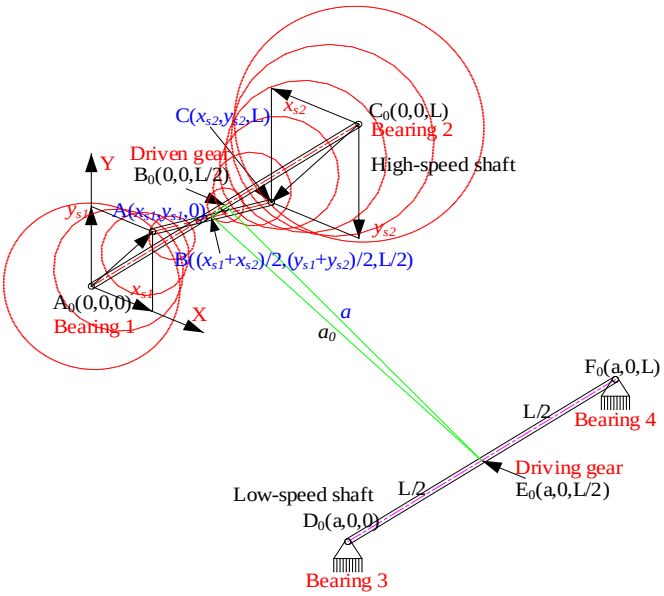


**Figure 2.** Gyroscopic motion of the high-speed shaft.

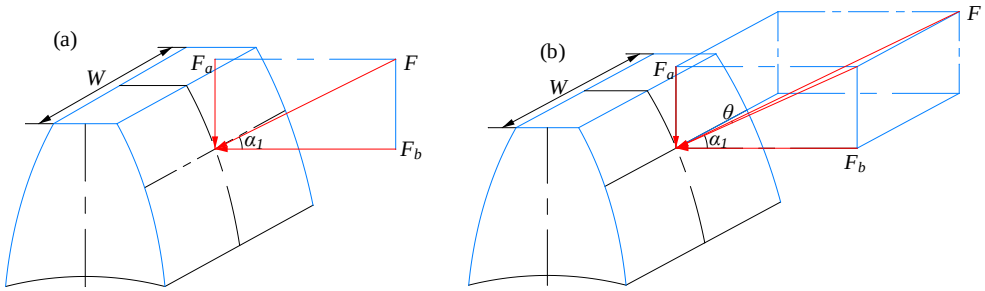


**Figure 3.** Direction of the meshing force: (a) Alignment; (b) Misalignment.

Bending deformation energy $U_b$:

$$U_b = \int_0^d \frac{[F_b(d-x) - F_a h]^2}{2EI_s} \mathrm{d}x = \frac{F^2}{2k_b}$$
$$= \int_{R_b}^{R_a} \frac{[F\cos\theta\cos\alpha_1\,(d-x) - F\cos\theta\sin\alpha_1\,h]^2}{2EI_s} \mathrm{d}x \quad (18)$$

Shear deformation energy $U_s$:

$$U_s = \int_0^d \frac{(1.2F_b)^2}{2GA_x} \mathrm{d}x = \frac{F^2}{2k_s} = \int_{R_b}^{R_a} \frac{(1.2F\cos\theta\cos\alpha_1)^2}{2GA_s} \mathrm{d}x \quad (19)$$

Radial compression deformation energy $U_a$:

$$U_a = \int_0^d \frac{F_a^2}{2EA_x} \mathrm{d}x = \frac{F^2}{2k_a} = \int_{R_b}^{R_a} \frac{(F\cos\theta\sin\alpha_1)^2}{2EA_s} \mathrm{d}x \quad (20)$$

Preprints (www.preprints.org) | NOT PEER-REVIEWED | Posted: 7 March 2022 doi:10.20944/preprints202203.0098.v1

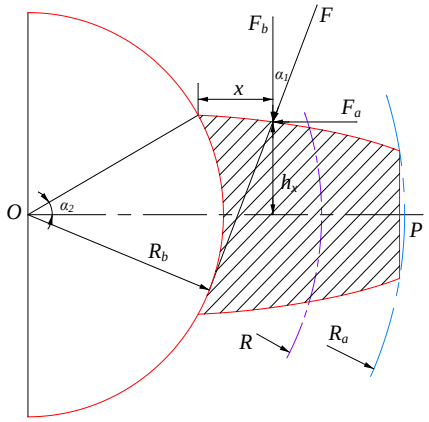


**Figure 4.** Beam model.

The load on the tooth surface is no longer evenly distributed, which causes torsional deformation of the tooth, as shown in Figure 5. Therefore, the torsional stiffness $k_\tau$ is generated, which can also be calculated based on the energy method.

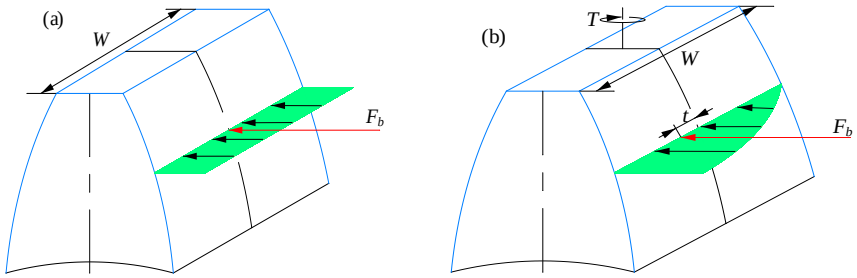


**Figure 5.** Load distribution: (a) Alignment; (b) Misalignment.

Torsional deformation energy $U_\tau$:

$$U_\tau = \int_0^d \frac{T^2}{2GI_{px}}\mathrm{d}x = \int_0^d \frac{(F_b \cdot t)^2}{2GI_{px}}\mathrm{d}x = \int_{R_b}^{R_a} \frac{(F\cos\theta\cos\alpha_1 \cdot t)^2}{2GI_{px}}\mathrm{d}x = \frac{F^2}{2k_\tau} \tag{21}$$

Where, $t$ represents the torsion arm, which can be calculated by the model in Ref. 36; $A_x$, $I_x$ and $I_{px}$ represent the cross-sectional area, the moment of inertia and the polar moment of inertia.

$$\begin{cases} A_s = 2h_xW \\ I_s = \dfrac{(2h_xW)^3}{12} \\ I_{px} = \dfrac{2h_xW}{12}(4h_x^2 + W^2) \end{cases} \tag{22}$$

Then, the stiffness components can be simplified to:

Shear stiffness $k_s$:

$$\frac{1}{k_s} = \int_{-\alpha_1}^{\alpha_2} \frac{1.2(1+v)(\alpha_2-\alpha)\cos\alpha\cos^2\alpha_1\cos^2\theta}{EW[\sin\alpha + (\alpha_2-\alpha)\cos\alpha]}\mathrm{d}\alpha \tag{23}$$

Bending stiffness $k_b$:

$$\frac{1}{k_b} = \int_{-\alpha_1}^{\alpha_2} \frac{3\left\{1+\cos\alpha_1[(\alpha_2-\alpha)\sin\alpha - \cos\alpha] - 2\cos\alpha_1\sin^2\frac{\theta}{2}\left[\begin{matrix}(\alpha_1+\alpha_2)\cos\alpha_1 - \sin\alpha \\ -(\cos\alpha - (\alpha_2-\alpha)\sin\alpha - \cos\alpha_2)\end{matrix}\right]\right\}^2}{2EW[\sin\alpha + (\alpha_2-\alpha)\cos\alpha]^3/[(\alpha_2-\alpha)\cos\alpha]}\mathrm{d}\alpha \tag{24}$$

Radial compression stiffness $k_a$:

Preprints (www.preprints.org) | NOT PEER-REVIEWED | Posted: 7 March 2022 doi:10.20944/preprints202203.0098.v1

$$\frac{1}{k_a} = \int_{-\alpha_1}^{\alpha_2} \frac{(\alpha_2-\alpha)\cos\alpha\sin^2\alpha_1\cos^2\theta}{2EW[\sin\alpha+(\alpha_2-\alpha)\cos\alpha]}\mathrm{d}\alpha \tag{25}$$

Torsional stiffness $k_\tau$:

$$\frac{1}{k_\tau} = \int_{-\alpha_1}^{\alpha_2} \frac{3L(1+v)(\alpha_2-\alpha)\cos^2\alpha_1\cos^2\theta\cos\alpha}{16E[\sin\alpha+(\alpha_2-\alpha)\cos\alpha]\{4R_b^2[\sin\alpha+(\alpha_2-\alpha)\cos\alpha]^2+W^2\}}\mathrm{d}\alpha \tag{26}$$

In addition, the actual center distance is considered, and the meshing principle of gear pairs is given:

$$r' = \frac{r\cos\alpha}{\cos\alpha'} \tag{27}$$

Where, $\alpha$ and $r$ is the pressure angle and pitch circle radius of the gear pair under standard installation; $\alpha'$ and $r'$ are the actual pressure angle and actual pitch circle radius during running. After $\alpha$ is replaced by $\alpha'$ in equation (18-26), the calculation of the meshing stiffness is completed. The stiffness $k_h$ and $k_f$ caused by contacting and body deformation can be quantified by the model in Ref. 37 and Ref. 38.

*2.5 Ball bearings with fitting clearances*

The model of ball bearings with fitting clearances is shown as Figure 6. Based on the assumptions in 1.1, a model of healthy bearings is established, as shown in Figure 6(a). When there are fitting clearances on bearings, the contact force between housing and outer ring is decomposed at the contact point, as shown in Figure 6(b). Also, the velocity of the outer ring is decomposed along the radial and normal directions, as shown in Figure 6(c).

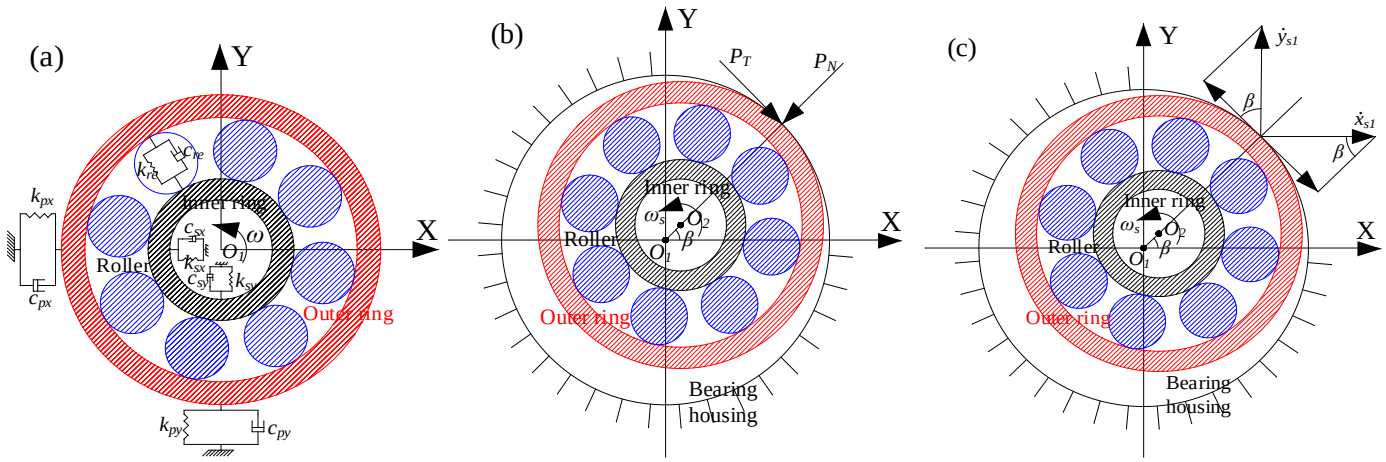


**Figure 6.** Bearing fitting clearance model: (a) Model of the ball bearing 1; (b) Force decomposition; (c) Velocity decomposition.

The bearing housing is fixed by bolts, and the radial displacement $r$ of the outer ring is:

$$r_p = x_{p1}\cos\beta + y_{p1}\sin\beta \tag{28}$$

When the radial displacement $r_p$ is less than the fitting clearance $\delta$, there is no contact between the housing and bearing, and the bearing is not supported by the housing.

$$\begin{cases} F_x = 0 \\ F_y = 0 \end{cases} \qquad \sqrt{x_{p1}^2 + y_{p1}^2} \le \delta \tag{29}$$

When $r_p$ is greater than $\delta$, the collision and friction will be caused. Then the tangential velocity $v_T$ of the outer ring is:

$$v_T = \dot{x}_{p1}\sin\beta + \dot{y}_{p1}\cos\beta \tag{30}$$

The angular position $\beta$ is satisfied the following equations:

Preprints (www.preprints.org) | NOT PEER-REVIEWED | Posted: 7 March 2022 doi:10.20944/preprints202203.0098.v1

$$\begin{cases} \sin\beta = \dfrac{y_{p1}}{r_p} = \dfrac{y_{p1}}{\sqrt{x_{p1}^2 + y_{p1}^2}} \\ \cos\beta = \dfrac{x_{p1}}{r_p} = \dfrac{x_{p1}}{\sqrt{x_{p1}^2 + y_{p1}^2}} \end{cases} \tag{31}$$

The nonlinear contact in Hertz theory [39] and Coulomb friction model are used to calculate the collision force $P_c$ and friction force $P_f$ generated by the fitting clearance.

$$\begin{cases} P_c = [\dfrac{(r-\delta)L_2^{0.8}}{3.83\times10^{-5}}]^{\frac{10}{9}} + c_N\dot{r} \\ P_f = f\cdot P_c\cdot \mathrm{sign}(v_T) \end{cases} \qquad \sqrt{x_{p1}^2 + y_{p1}^2} > \delta \tag{32}$$

Where, $f$ represents the coefficient of friction; $c_N$ represents the damping coefficient.

After simplification, the excitation force caused by the fitting clearance can be described as:

$$\begin{pmatrix} F_x \\ F_y \end{pmatrix} = \begin{pmatrix} \dfrac{x_{p1}}{\sqrt{x_{p1}^2 + y_{p1}^2}} & \dfrac{f\cdot y_{s1}\cdot \mathrm{sign}(\dot{x}_{p1}\cdot y_{p1} + \dot{y}_{p1}\cdot x_{p1})}{x_{p1}^2 + y_{p1}^2} \\ \dfrac{y_{p1}}{\sqrt{x_{p1}^2 + y_{p1}^2}} & \dfrac{f\cdot x_{s1}\cdot \mathrm{sign}(\dot{x}_{p1}\cdot y_{p1} + \dot{y}_{p1}\cdot x_{p1})}{x_{p1}^2 + y_{p1}^2} \end{pmatrix}_{2\times2} \begin{pmatrix} [\dfrac{(x_{p1}^2 + y_{p1}^2 - \delta\cdot\sqrt{x_{p1}^2 + y_{p1}^2})L_2^{0.8}}{3.83\times10^{-5}\cdot\sqrt{x_{p1}^2 + y_{p1}^2}}]^{\frac{10}{9}} + \dfrac{c_N\cdot(\dot{x}_{p1}\cdot y_{p1} + \dot{y}_{p1}\cdot x_{p1})}{\sqrt{x_{p1}^2 + y_{p1}^2}} \\ [\dfrac{(x_{p1}^2 + y_{p1}^2 - \delta\cdot\sqrt{x_{p1}^2 + y_{p1}^2})L_2^{0.8}}{3.83\times10^{-5}\cdot\sqrt{x_{p1}^2 + y_{p1}^2}}]^{\frac{10}{9}} + \dfrac{c_N\cdot(\dot{x}_{p1}\cdot y_{p1} + \dot{y}_{p1}\cdot x_{p1})}{\sqrt{x_{p1}^2 + y_{p1}^2}} \end{pmatrix}_{2\times1} \tag{33}$$

When there are fitting clearances on bearings, the housing has no supporting effect on the outer ring. However, the outer ring is supported by the collision force and friction force, and the following equations are set.

$$\begin{cases} k_{px} = k_{py} = 0 \\ c_{px} = c_{py} = 0 \end{cases} \tag{34}$$

## 3. Results and discussion

The model of gear-rotor-bearing systems with bearing fitting clearances can be solved by using the $Runge-Kutta$ method in $matlab$. The parameter of the dynamic model is shown in Table 1, and the bearing types are listed as in Table 2, where the defect frequencies are added. The parameters of gear pairs are selected in Table 3. It is assumed that there are fit clearances between outer ring and housing in bearing 1, and other bearings are healthy. After the numerical solution is obtained, the dynamic response of resonators is extracted for analysis.

### *3.1 Influence of bearing fitting clearances on the gear-rotor-bearing system*

#### *3.1.1 The center distance error and offset angle of the gear pair*

When there are fitting clearances between housing and outer ring, the stablished dynamic model is solved, then the center distance error and offset angle of gear pairs can be obtained, as shown in Figure 7. It is found that the bearing fitting clearances have a great effect on the actual center distance and offset angle of gear pairs. The center distance error is shown in Figure 7(a), and when there are fitting clearances on bearings, the local peak value in the center distance error curve is not increased drastically. The affected center distance error curve is fluctuating up and down, and the frequency of the envelope is the defect frequency $f_{o1}$. With the increase of bearing fitting clearances, the amplitude modulation in

Preprints (www.preprints.org) | NOT PEER-REVIEWED | Posted: 7 March 2022 doi:10.20944/preprints202203.0098.v1

the center distance error curve is intensified, the fluctuation is more severe. In addition, the phase of the center distance error curve is constantly advanced due to the increased bearing clearance. The offset angle of gear pairs is shown in Figure 7(b). When there are bearing fitting clearances between housing and outer ring, the local peak value in the offset angle curve is significantly increased, and it is also influenced by the amplitude modulation of the bearing outer ring, which also makes the curve fluctuate up and down.

**Table 1.** Parameters of the dynamic model.

| Parameters/(unit) | Values | Parameters/(unit) | Values |
|---|---|---|---|
| Moment of inertia of input shaft $I_{f1}/(kg \cdot m^2)$ | 0.0021 | Torsional stiffness of shaft $k_{f1}, k_{f2}$ $/(Nm/rad)$ | $4.4e^5$ |
| Moment of inertia of driving gear $I_{pin}/(kg \cdot m^2)$ | $4.365e^{-4}$ | Torsional damping of shaft $c_{f1}, c_{f2}/(Nms/rad)$ | $5e^5$ |
| Moment of inertia of driven gear $I_{ge}/(kg \cdot m^2)$ | $8.362e^{-4}$ | Support stiffness of bearings $k_{sj}, k_{pj}$ , $k_{rj}/(N/m)$ | $6.56e^7$ |
| Moment of inertia of output shaft $I_{f2}/(kg \cdot m^2)$ | 0.0105 | Support damping of bearings $c_{sj}, c_{pj}, c_{rj}/(Ns/m)$ | $1.8e^5$ |
| Load (N/m) | 25 | Connection stiffness $k_{o1}/(N/m)$ | $6.56e^7$ |
| Mass of driving gear $m_{pin}/kg$ | 0.96 | Damping coefficient $c_N/(Ns/m)$ | $2e^5$ |
| Mass of driven gear $m_{ge}/kg$ | 2.88 | Length of shafts $L/mm$ | 260 |
| Average transmission fluctuation $e_o/m$ | $3e^{-5}$ | Friction coefficient $f$ | 0.1 |
| Transmission fluctuation range $e_m/m$ | $2e^{-5}$ | Rotation frequency of input shaft $f_{r1}/Hz$ | 30 |

**Table 2.** Bearing types.

| Bearings | Types | Defect frequency of the outer raceway $f_o/Hz$ | Defect frequency of the inner raceway $f_i/Hz$ |
|---|---|---|---|
| Bearing 1 | 6304 | 81.13 | 132.79 |
| Bearing 2 | 6304 | 81.13 | 132.79 |
| Bearing 3 | 6308 | 21.92 | 37.71 |
| Bearing 4 | 6308 | 21.92 | 37.71 |

**Table 3.** Parameters of gear pairs.

| Parameters/(unit) | High-speed gear | Low-speed gear |
|---|---|---|
| Modulus $m/mm$m / (mm) | 2 | 2 |
| Pressure Angle $\alpha/(°)$$\alpha_0$ / (∘) | 20 | 20 |
| Number of teeth $z$z | 23 | 81 |
| Young's modulus $E/GPa$ | 216 | 216 |
| Tooth width $W/mm$L / (mm) | 24 | 24 |

In gear-rotor-bearing systems, the actual center distance and offset angle of gear pairs are severely affected by bearing fitting clearances, which makes the high-speed shaft perform more violent gyroscopic motion. However, the gear pair is generally installed at the midpoint of shafts, the offset angle is greatly affected by bearing fitting clearances, and the change in actual center distance is relatively small. The main form of influence is amplitude modulation.

Preprints (www.preprints.org) | NOT PEER-REVIEWED | Posted: 7 March 2022 doi:10.20944/preprints202203.0098.v1

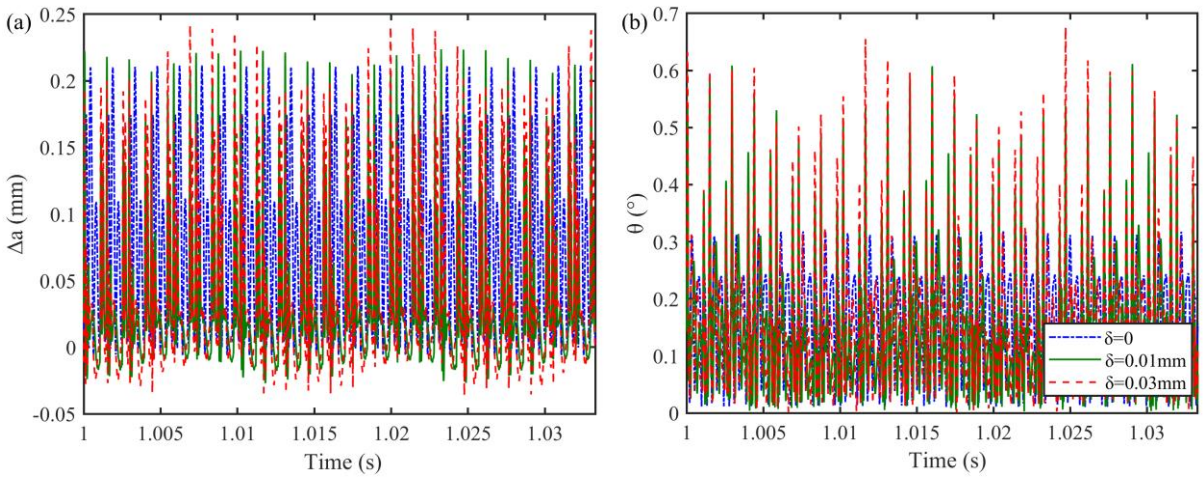


**Figure 7.** Center distance error and offset angle: (a) Center distance error; (b) Offset angle.

*3.1.2 Meshing stiffness of gear pairs*

The calculated meshing stiffness excitation of gear pairs is extracted, the result is shown in Figure 8. When there are bearing fitting clearances in systems as shown in Figure 8(a), the meshing stiffness is generally reduced, and it is affected by the amplitude modulation of the bearing outer ring, and the multiple local extremes of the meshing stiffness are caused. The distribution of these local extremes is mostly concentrated on the start point and end point of the single-tooth and double-tooth meshing interval, and the trend of the extremes is more complicated as the fitting clearance increases.

When the fitting clearance is 0.01mm, 0.02mm and 0.03mm, the meshing stiffness curves are extracted for comparison, the result is shown in Figure 8(b). In general, the reduction in meshing stiffness is caused, and it is modulated by $f_{o1}$. Moreover, the modulation phenomenon becomes more serious as the bearing fitting clearance increases. The meshing stiffness in single-tooth meshing interval of gear pairs is shown in Figure 8(c). The minimum meshing stiffness is continuously reduced. In particular, the meshing stiffness curve is no longer strictly periodic, which seriously affects the nonlinear dynamic characteristics of gear pairs.

*3.1.3 Time-domain response*

The displacement response of bearing 1 resonator in the gear-rotor-bearing system is shown in Figure 9. When there is no fitting clearance or the fitting clearance is small on the bearing as shown in Figure 9(a), the response of gear-rotor-bearing systems is still stable. As the fitting clearance increases, the displacement time-domain response of the gearbox is fluctuated due to the amplitude modulation, and the degree of fluctuations is increased. The displacement responses of the gear-rotor-bearing system with bearing fitting clearances of 0.01mm, 0.03mm and 0.05mm are extracted and plotted as Figure 9(b). It is found that the dynamic response of the gearbox is fluctuated significantly, and the maximum value of the displacement is continuously increased with the increase of fitting clearances. The median line of each displacement curve is extracted and drawn as Figure 9(c). It is can be seen that the amplitude modulation of the outer ring will be exacerbated as the fitting clearance

Preprints (www.preprints.org) | NOT PEER-REVIEWED | Posted: 7 March 2022 doi:10.20944/preprints202203.0098.v1

increases, the fluctuation trend becomes more serious, and the frequency interval between adjacent peaks is the defect frequency $f_{o1}$.

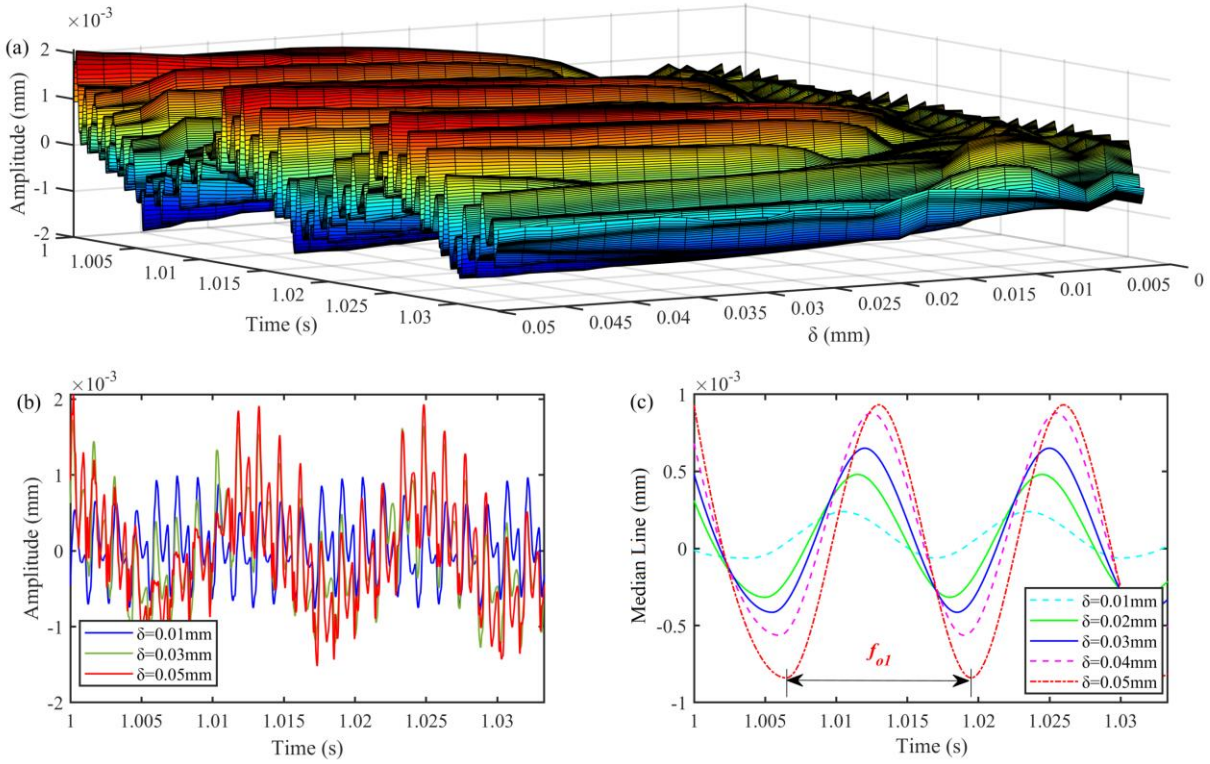


**Figure 9.** Time-domain response of gear-rotor-bearing systems: (a) Time-domain displacement response; (b) Comparison of displacement response with the fitting clearance of 0.01mm, 0.03mm and 0.05mm; (c) The median line of the displacement response.

*3.1.4 Frequency-domain response*

After the Fast Fourier Transform, the frequency-domain response can be acquired, as shown in Figure 10. From the low frequency band (0-2500Hz) of the spectrogram in Figure 10(a), it is found that there are the defect frequency and the multiple harmonic frequency of the bearing outer raceway, such as $10f_{o1}, 11f_{o1}, 12f_{o1}, 18f_{o1}$. It shows that the multiple harmonic response of the bearing outer raceway is generated due to the fitting clearance. As the fitting clearance increases, the higher-order multiple harmonic response will be excited. In addition, there are also meshing frequencies of gear pairs on the spectrum, such as $f_m, 2f_m, 3f_m$, and the defect frequency of gear pairs is also found on the spectrum due to the periodic deterioration of the meshing stiffness, such as $f_m \pm f_{r1}, 2f_m \pm f_{r1}, 3f_m \pm f_{r1}$.

The high frequency band (2500-5000Hz) of the spectrum is given as Figure 10(b). In this high frequency band, the spectrum is composed of multiple harmonic frequencies of the meshing frequency, such as $4f_m, 5f_m, 6f_m, 7f_m$, which means that the multiple harmonic response of gear pairs is generated by the fitting clearance. As the fitting clearance increases, higher-order multiple harmonic response will be excited. Besides, there are obvious harmonic frequencies generated by the frequency modulation on both sides of the multiple harmonic frequencies of the gear pair, such as $4f_m \pm f_{r1}, 5f_m \pm f_{r1}, 6f_m \pm f_{r1}, 7f_m \pm f_{r1}$, and the amplitude of the harmonic frequency is also increased as the increased fitting clearance.

Preprints (www.preprints.org) | NOT PEER-REVIEWED | Posted: 7 March 2022 doi:10.20944/preprints202203.0098.v1

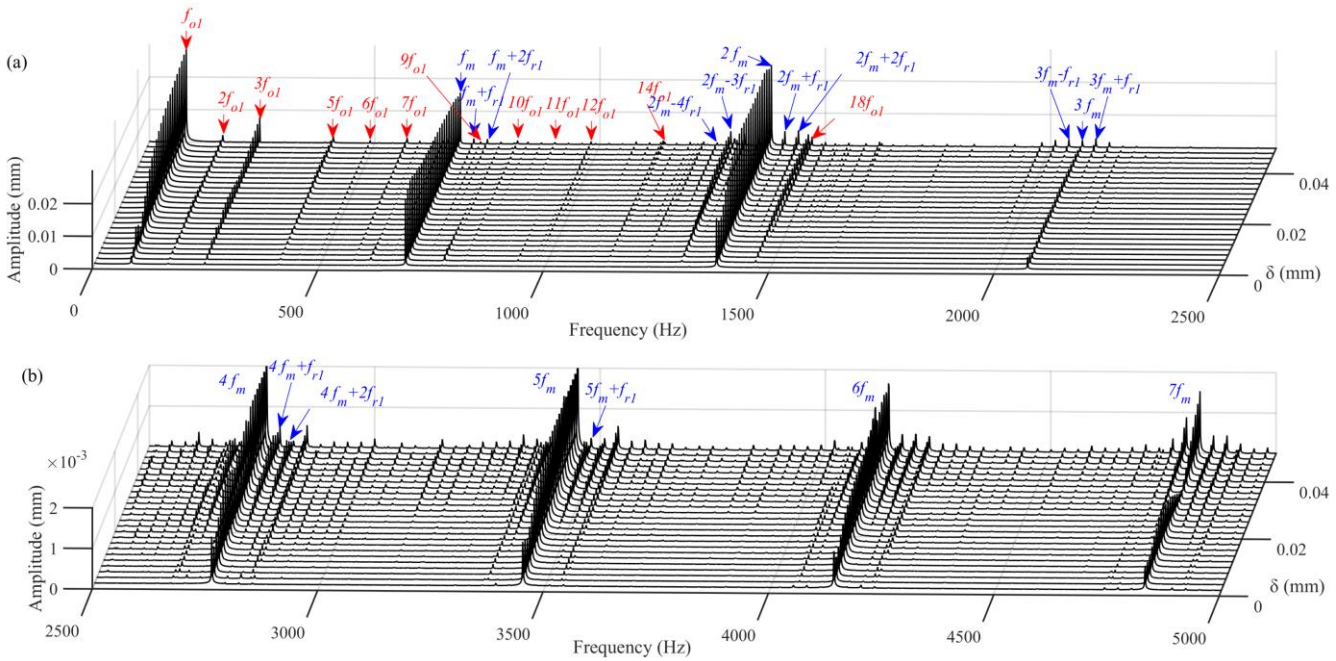


**Figure 10.** Frequency-domain response of gear-rotor-bearing systems: (a) Low frequency band; (b) High frequency band.

The amplitude of $f_m$ and $f_{o1}$ in Figure 10 is extracted and plotted as Figs 11. The change in the amplitude of $f_m$ is shown in Figure 11(a). When the supporting bearing is healthy, there are mainly the fundamental frequency $f_m$ and the second harmonic frequency $2f_m$ on the spectrum, and the amplitude of higher-order multiple harmonic frequencies is extremely small and can be ignored. When the bearing fitting clearance is 0 to 0.005mm, the amplitude of $f_m$ is continuously increased, and the amplitude of $2f_m$ is reduced instead. This shows that when the bearing clearance is small, although the vibration amplitude of the gear pair is increased, the relationship between bearings and gear pairs is strengthened, and under the action of the tiny fitting clearance, the gear pair mainly vibrates at fundamental frequency.

When the bearing fitting clearance is about 0.005mm, there is an inflection point on the amplitude curve of the meshing frequency, the amplitude of the fundamental frequency $f_m$ reaches the maximum value, and the amplitude of $2f_m$ reaches the minimum value. When the bearing clearance changes from 0.005mm to 0.045mm, the amplitude of the fundamental frequency $f_m$ is continuously reduced, on the contrary, the amplitude of the second multiple harmonic frequency $2f_m$ is continuously increased. In this bearing fitting clearance range, the center distance and offset angle of shaft are deteriorated, and the gear pair mainly vibrates at the second multiple harmonic frequency. In addition, the amplitude of $2f_m$ is greater than $f_m$, this indicates that the gear pair is running with serious center distance error and offset angle. When the bearing clearance is 0.045mm, the amplitude of $2f_m$ reaches the maximum. Then, the amplitude of $2f_m$ and $f_m$ begin to decrease. However, the amplitude of the higher-order multiple harmonics of the meshing frequency is consistently increasing, which shows that the gear pair is developing to vibrate at the higher-order multiple harmonics frequency.

Preprints (www.preprints.org) | NOT PEER-REVIEWED | Posted: 7 March 2022 doi:10.20944/preprints202203.0098.v1

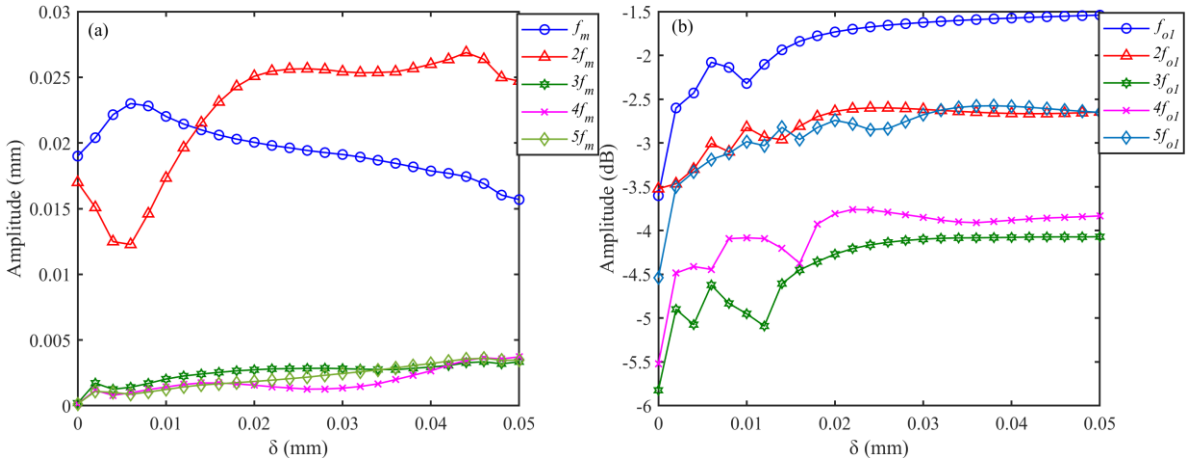


**Figure 11.** The changes in amplitude: (a) $f_m$; (b) $f_{o1}$.

The amplitude of $f_{o1}$ is shown in Figure 11(b). The changes in the amplitude of $f_{o1}$ are extremely complicated when the fitting clearance is less than 0.015mm, and the multiple harmonics of $f_{o1}$ are generated. When the fitting clearance is greater than 0.015mm, the amplitude of multiple harmonic frequencies is changed regularly, and an increasing trend is shown. In general, the amplitude of the fundamental frequency $f_{o1}$ is the largest, which shows that the bearing still mainly vibrates at fundamental frequency.

It can be summarized that the multiple harmonic response of the bearing outer ring and the gear pair will be generated by the bearing fitting clearance, and the change in their amplitude is more sensitive when the bearing fitting clearance is small.

*3.1.5 Displacement of high-speed shaft*

The vibration characteristics of bearings and gear pairs in gear-rotor-bearing systems with bearing fitting clearances have been analyzed, then the dynamic response is further discussed from the perspective of shaft displacement, the result is shown in Figure 12. The axis track of the high-speed shaft at the end of bearing 1 is drawn as Figure 12(a), since the meshing process of gear pairs can actually be regarded as a periodic collision behavior, coupled with the collision between housing and outer ring in the bearing with fitting clearances, which causes the axis track to be chaotic and disorderly. When there is no clearance in the bearing, the axis track of the high-speed transmission shaft is stayed in a certain area. The vibration of gearboxes in the y direction is excited by the meshing force of gear pairs and the contact force of bearings, while the vibration in the x direction is only excited by the contact force of the bearing, which causes the shaft displacement in the y direction to be larger than the displacement in the x direction, and makes the graph of the axis track close to the shape of an ellipse. After there are fitting clearances in bearings. the displacement of the high-speed shaft in both the x and y directions is increased. However, the meshing force is severely affected by the fitting clearance, causing the increase in the shaft displacement in the y direction to be greater than the increase in the x direction. And when the fitting clearance is increased, the displacement increase in the y direction is more obvious.

A period of the axis track in Figure 12(a) is mapped to polar coordinates, as shown in Figure 13(b). The collision will be generated when the tooth enters meshing, then the sudden change of bearing displacement is generated, it is quickly attenuated under the action of

Preprints (www.preprints.org) | NOT PEER-REVIEWED | Posted: 7 March 2022 doi:10.20944/preprints202203.0098.v1

elastic restoring force when there is no fitting clearance, and the attenuation process is carried out once or a few times. Therefore, there is less shock on the displacement response curve of the gearbox, which causes gear pair to be vibrate at fundamental frequencies mainly. When there is a fitting clearance and as the clearance increases, the displacement of the high-speed shaft is significantly increased. The displacement is converged after multiple attenuation processes, which causes the number of shocks to be increased and leads to more peaks in polar coordinates. The number of peaks is related to the gear pair and bearing, which is also the main reason why the multiple harmonic response of the gear pair and bearings are generated.

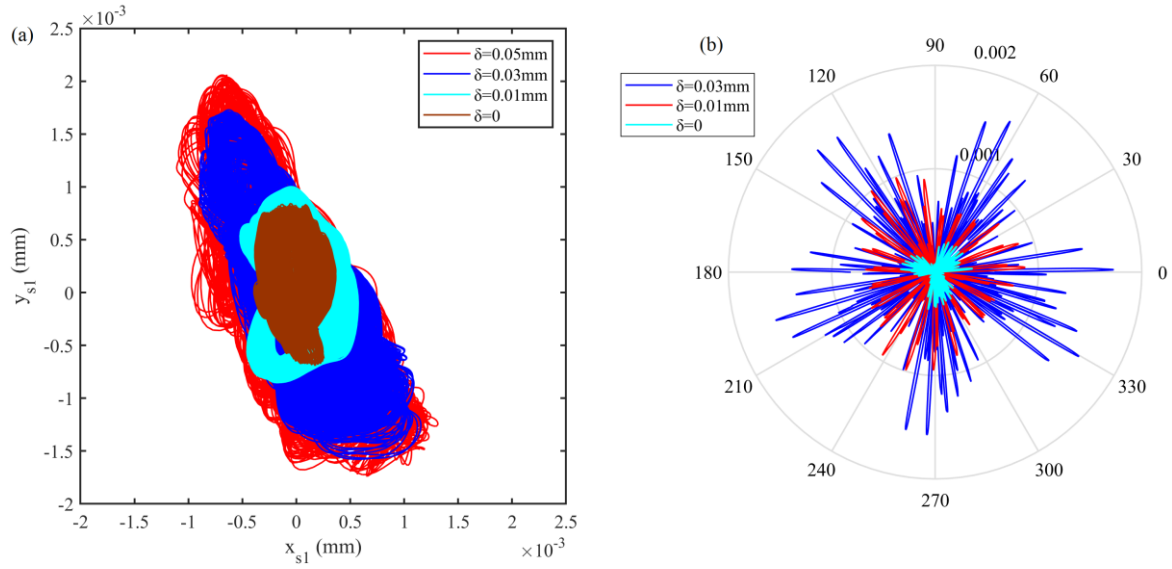


**Figure 12** Displacement of the high-speed shaft: (a) Axis track; (b) Mapped to the polar coordinate.

*3.2 The influence of speed on gear-rotor-bearing systems with bearing fitting clearances*

The fitting clearance between housing and outer ring in bearing 1 is set to 0.02mm, by setting different speeds, the dynamic response of gear-rotor-bearing systems with bearing fitting clearances is further studied.

*3.3.1 Meshing stiffness of gear pairs*

The meshing stiffness when the gear-rotor-bearing system is operated at different speeds is presented in Figure 13. It can be seen that when the input speed is increased, the amplitude modulation of the bearing outer ring to the meshing stiffness will be enhanced, and the degree of curve fluctuation is further increased. In gear-rotor-bearing systems, due to the increase in the input speed, the more violent gyroscopic movement of shafts is caused, which seriously affects the offset angle and actual center distance of gear pairs, and makes the meshing process more chaotic.

*3.2.2 Vibration responses*

When the gear-rotor-bearing systems work at different input speeds, the dynamic response is shown in Figure 14. The time-domain dynamic response is displayed in Figure 14(a), it is found that as the input speed increases, the amplitude of the response will be further increased, and the amplitude modulation will be enhanced. Then the *RMS* (Root Mean Square) and $x_{p-p}$ (Peak-to-Peak Values) methods of mathematical statistics are used

Preprints (www.preprints.org) | NOT PEER-REVIEWED | Posted: 7 March 2022 doi:10.20944/preprints202203.0098.v1

to process the dynamic response, and the results are shown in Figure 14(b). As the input speed increases, the *RMS* and $x_{p-p}$ of the time-domain response are shown to be constantly increasing.

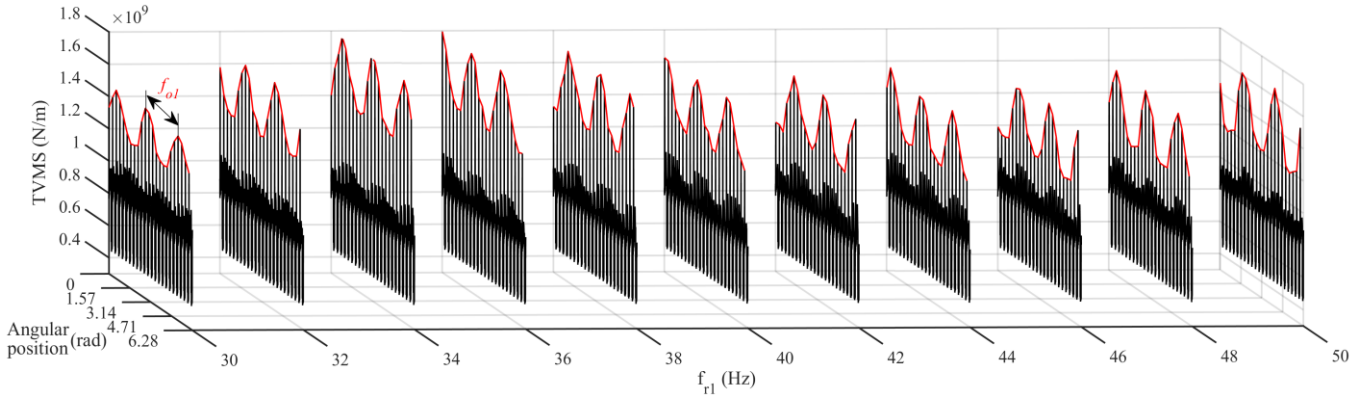


**Figure 13.** Meshing stiffness of gear pairs at different input speeds.

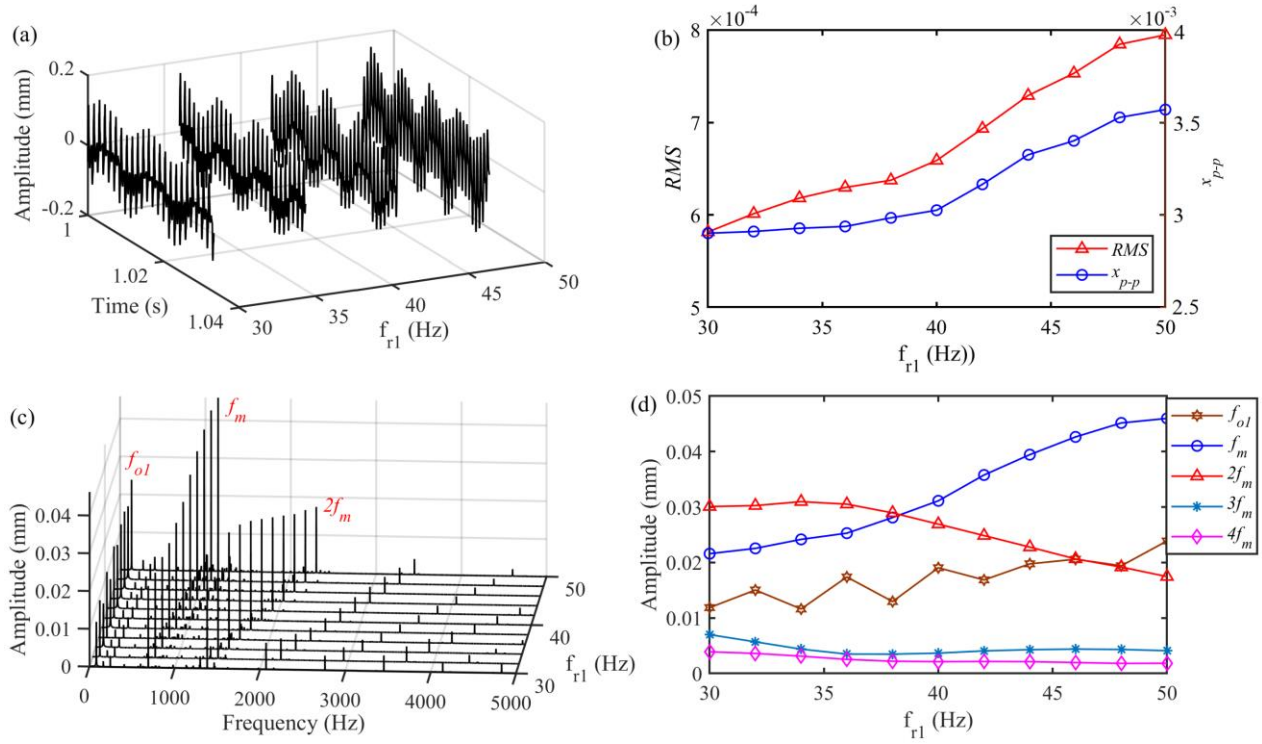


**Figure 14.** Response of gear-rotor-bearing systems at different input speeds: (a) Time-domain response; (b) *RMS* and $x_{p-p}$; (c) Frequency-domain response; (d) Amplitude of $f_m$ and $f_{o1}$.

Figure 14(c) shows the frequency-domain response. The spectrum is still mainly composed of the defect frequency $f_{o1}$ and the meshing frequency $f_m$. On both sides of $f_m$ and $2f_m$, a large number of harmonic frequencies of gear pairs are generated. On the contrary, there are almost no harmonic frequencies on both sides of $3f_m$, $4f_m$, $5f_m$, which shows that when the speed is increased, the high-order harmonic frequencies of the gear pair are suppressed, and the harmonic frequencies caused by frequency modulation is more likely to be generated around the low-order multiple harmonics of the meshing frequency. In the high

Preprints (www.preprints.org) | NOT PEER-REVIEWED | Posted: 7 March 2022 doi:10.20944/preprints202203.0098.v1

frequency band, except for the meshing frequencies, the defect frequencies $f_{o1}$ can hardly be found, which means that as the input speed increases, the multiple harmonic response of the outer raceway is weakened, and the bearing mainly vibrate at the fundamental frequency.

The amplitude of meshing frequencies $f_m$ and defect frequencies $f_{o1}$ are extracted and plotted as Figure 14(d). It is found that as the input speed increases, the amplitude of $f_{o1}$ is continuously increased, and the vibration of bearing outer rings is intensified. However, the amplitude of the fundamental frequency $f_m$ is increased, and the amplitude of multiple harmonic frequencies are reduced. This indicates that the multiple harmonic response of gear pairs is suppressed by increasing the speed, and the relationship between bearings and gear pairs is weakened.

It can be concluded from the above response analysis that when the input speed of gear-rotor-bearing systems with bearing fitting clearances is increased, the vibration is heightened, and the modulation caused by bearing fitting clearances will be more obvious. However, the multiple harmonic response of bearings and gear pairs is suppressed, and the connection between bearings and gear pairs is weakened, which makes the gear-rotor-bearing system more prone to vibrate at the fundamental frequency.

## 4. Experimental verification

Through the established model, the response analysis of gear-rotor-bearing systems with fitting clearances is completed. Next, the dynamic response of gearboxes is also analyzed by experimental method, which can be used to validate the model.

The test-bed shown in Figure 15(a) is used for experiments, the supporting bearing with fitting clearances is shown in Figure 15(b), and the fitting clearance is set to 0.02mm. The component and parameter used in the experiment are consistent with the model settings. The vibration response at the bearing end caps is measured by the accelerometer, and the sampling frequency is set to 30k Hz, then the dynamic response in the plumb direction is collected for vibration analysis.

After the experiment, the response of the gearbox can be obtained as shown in Figs 16. The gear-rotor-bearing system model with bearing fitting clearances is solved, and the numerical solutions of $\ddot{y}_{b1}$ are given as Figure 16(a) and Figure 16(b), and the response obtained from the experiment is shown in Figure 16(c) and 16(d). It can be seen from Figure 16(c) that the time-domain response of the gearbox is modulated by the defect frequency $f_{o1}$ of bearing outer raceway, and the frequency of the shock is the defect frequency $f_{o1}$. As shown in Figure 16(d), the spectrum is mainly composed by the defect frequencies $f_{o1}$ and the meshing frequencies, as well as the multiple harmonic frequencies of bearings and gear pairs, such as $3f_m, 4f_m, 5f_m, 6f_m, 7f_m, 4f_{o1}, 5f_{o1}, 6f_{o1}$, which can explain that the multiple harmonic response of gear pairs and bearings can be excited by bearing fitting clearances. In addition, there are harmonic frequencies $f_m \pm f_{r1}, 2f_m \pm f_{r1}, 3f_m \pm f_{r1}$ of gear pairs on the spectrum, which prove that the bearing fitting clearances have motivating effects on the meshing stiffness, and there are coupling relationships between bearings and gear pairs. By comparing the experimental results with the simulation results, the dynamic model and the vibration analysis are verified.

Preprints (www.preprints.org) | NOT PEER-REVIEWED | Posted: 7 March 2022 doi:10.20944/preprints202203.0098.v1

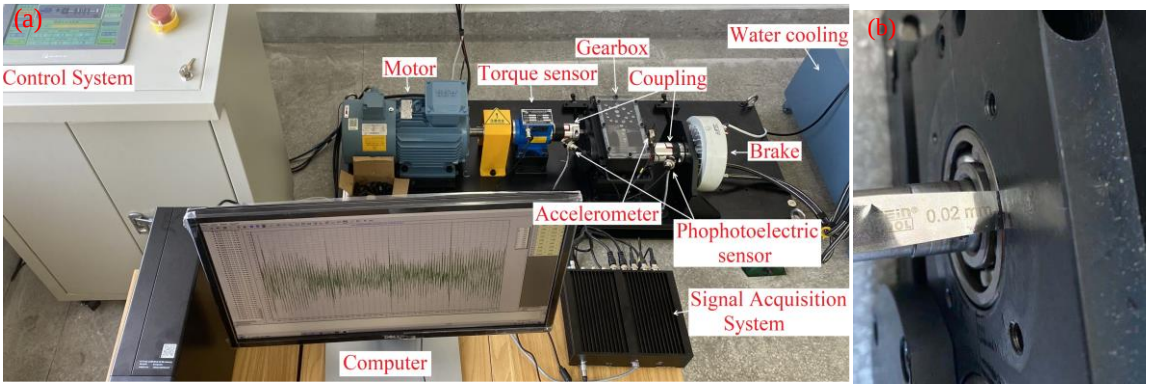


**Figure 15.** Equipment: (a) Gear-rotor-bearing system test-bed; (b) Bearing with fitting clearances.

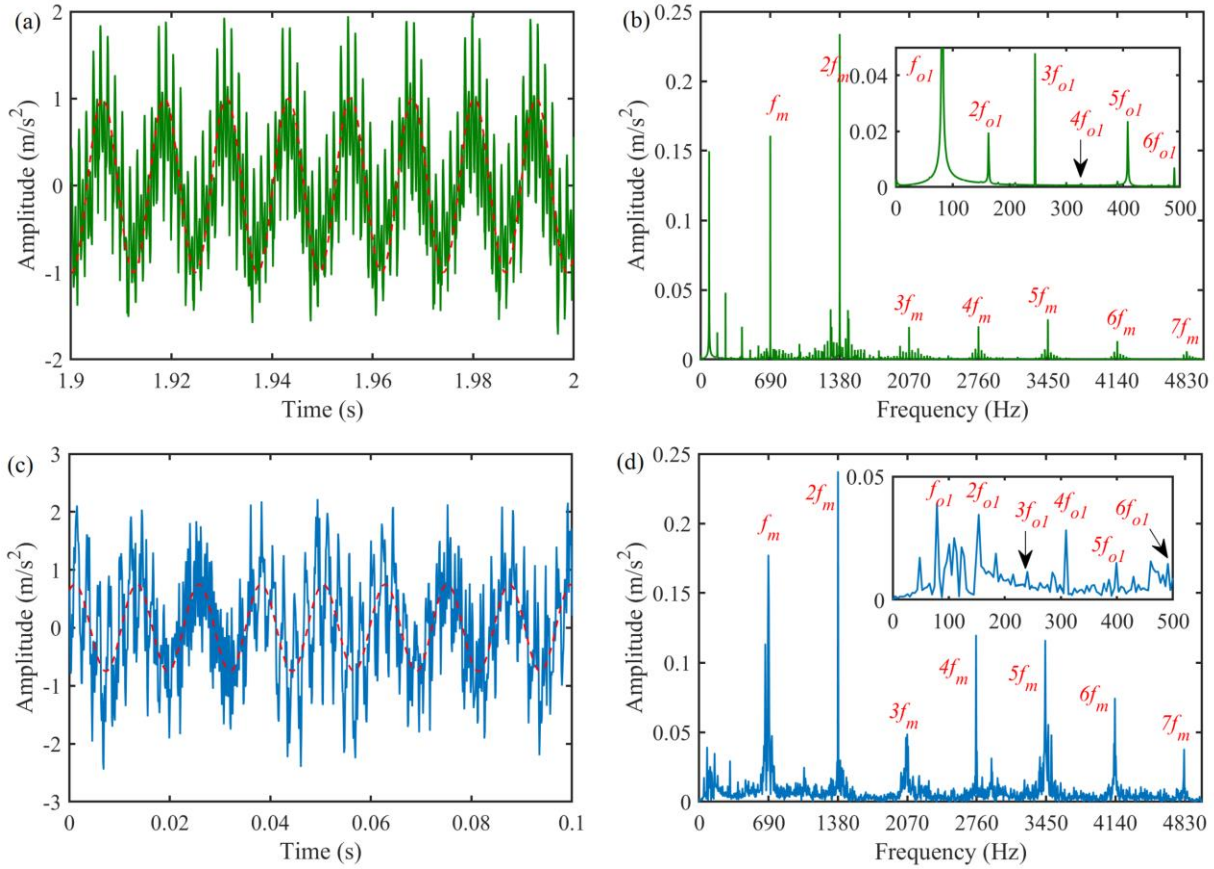


**Figure 16.** Response of the gearbox: (a) Time-domain response obtained by the established model; (b) Frequency-domain response obtained by the established model; (c) Time-domain response obtained by the experiment; (d) Frequency-domain response obtained by the experiment.

## 5. Conclusion

For realizing the vibration analysis of gear-rotor-bearing systems with bearing fitting clearances, a dynamic model of gear-rotor-bearing systems with bearing fitting clearances is established, in which the bearing and gear pair are combined, and the vibration transmission between bearings and gear pairs is determined. The fitting clearances between outer ring and housing in bearings are considered, as well as the friction force and collision force caused by fitting clearances, which are calculated by Coulomb friction model and the Hertz theory. Then

the influences of bearing fitting clearances on dynamic characteristics of gear-rotor-bearing systems are studied. Some results are summarized as follows:

(1) When there are fitting clearances on the bearing, the amplitude modulation of the bearing outer raceway to the system time-domain response is exacerbated, and the multiple harmonic frequency of bearings and gear pairs are generated on the spectrum, as well as defect frequencies of gear pairs. As the fitting clearance is increased, the higher multiple harmonic responses will be caused.

(2) Although the response amplitude of the gearbox is increased by raising the input speed, multiple harmonic responses are suppressed, which makes the system mainly vibrate at the fundamental frequency.

(3) The dynamic model and the vibration analysis are experimentally verified.

**Author Contribution:** Peng Dai: Writing – original draft, Investigation. Jianping Wang: Conceptualization, Visualization, Validation. Linkai Niu: Resources, Methodology, Multiplevision. Fengtao Wang: Project administration, Writing – review & editing.

**Funding:** This paper was supported by the National Natural Science Foundation of China (No. 51905001) and Wuhu Science and Technology Projects (No. 2020yf53).

**Institutional Review Board Statement:** Not applicable.

**Informed Consent Statement:** Not applicable.

**Data Availability Statement:** Not applicable.

**Conflicts of Interest:** The authors declare no conflict of interest.

## References

1. Song CH, Bai H, Zhu CC, Wang YW, Feng ZH, Wang Y. Computational investigation of off-sized bearing rollers on dynamics for hypoid gear-shaft-bearing coupled system. Mechanism and Machine Theory 2021; 156: 104177.
2. Xu MM, Han YY, Sun XQ, Shao YM. Vibration characteristics and condition monitoring of internal radial clearance within a ball bearing in a gear-shaft-bearing system. Mechanical Systems and Signal Processing 2022; 165.
3. Visnadi Laís Bittencourt, de Castro Helio Fiori. Influence of bearing clearance and oil temperature uncertainties on the stability threshold of cylindrical journal bearings. Mechanism and Machine Theory; 2019: 134; 57-73.
4. Krot Pavlo, Korennoi Volodymyr, Zimroz Radoslaw. Vibration-Based Diagnostics of Radial Clearances and Bolts Loosening in the Bearing Supports of the Heavy-Duty Gearboxes. Sensors 2020; 20.
5. Liu J, Ding SZ, Wang LF, Xu J. Effect of the bearing clearance on vibrations of a double-row planetary gear system. Proceedings of the Institution of Mechanical Engineers, Part K: Journal of Multi-body Dynamics 2020; 234: 347-357.
6. Y Yang, WK Xia, JM Han, YF Song, JF Wang, YP Dai. Vibration analysis for tooth crack detection in a spur gear system with clearance nonlinearity. International Journal of Mechanical Sciences 2019; 157-158: 648-661.
7. L Zhang, H Xu, SL Zhang, SY Pei. A radial clearance adjustable bearing reduces the vibration response of the rotor system during acceleration. Tribology International 2020; 144(C): 106112-106112.
8. RL Zhang, KD Wang, YD Shi, XQ Sun, T Wang. The Influences of Gradual Wears and Bearing Clearance of Gear Transmission on Dynamic Responses. Energies, 2019, 12(24).
9. Fingerle Andreas; Hochrein Jonas; Otto Michael; Stahl Karsten. Theoretical Study on the Influence of Planet Gear Rim Thickness and Bearing Clearance on Calculated Bearing Life. Journal of Mechanical Design 2020; 142.
10. Tallian T E, Gustafsson O G. Progress in Rolling Bearing Vibration Research and Control. A S L E Transactions 1965; 8: 195-207.
11. Kahraman A. Load Sharing Characteristics of Planetary Transmissions. Mech. Mach. Theory 1994; 29: 1151-1165.

12. Kahraman A, Singh R. Interactions between Time-Varying Mesh Stiffness and Clearance Non-Linearities in a Geared System. J. Sound Vib 1991; 146: 135-156.
13. Guo Y, Parker R G. Dynamic Analysis of Planetary Gears with Bearing Clearance. J. Comput. Nonlinear Dyn 2012; 7.
14. Chen XH, Yang CK, Zuo MJ, Tian ZG. Planetary Gearbox Dynamic Modeling Considering Bearing Clearance and Sun Gear Tooth Crack †. Sensors 2021; 21: 2638-2638.
15. Tomović R. Calculation of the necessary level of external radial load for inner ring support on the rolling elements in a radial bearing with internal radial clearance. International Journal of Mechanical Science 2012; 60:37-39.
16. Inagaki M, Ishida Y. Mechanism of Occurrence of Self-Excited Oscillations of a Rotor with a Clearance between Bearing Holder and Housing. Volume 1: 23rd Biennial Conference on Mechanical Vibration and Noise, Parts A and B, 2011.
17. M Tiwari K. Gupta. Effect of radial internal clearance of a ball bearing on the dynamics of a balanced horizontal rotor. Journal of Sound and Vibration 2000; 238:723-756.
18. Chu F. Tang Y. Stability and Non-linear responses of a rotor-bearing system with pedestal looseness． Journal of Sound and Vibration 2001; 241(5):879-893.
19. Behzad M, M. Asayeshthe. Numerical and experimental investigation on vibration of rotors with loose disks. Proceedings of the Institution of Mechanical Engineers, Part C: Journal of Mechanical Engineering Science 2010; 223:1-10.
20. W Lu, F Chu. Experimental investigation of pedestal looseness in a rotor-bearing system. Key Engineering Materials 2009; 413-414:599-605.
21. Ma H, Zeng J, Feng R, Pang X, Wang Q, Wen B. Review on dynamics of cracked gear systems. Engineering Failure Analysis 2015; 55: 224-245.
22. Ian Howard, SX Jia. The dynamic modeling of a spur gear in mesh including friction and a crack. Mechanical Systems and Signal Processing 2001; 15(5):831-853.
23. Parey A, El Badaoui M, Guillet F, Tandon N. Dynamic modelling of spur gear pair and application of empirical mode decomposition-based statistical analysis for early detection of localizedized tooth defect. Journal of Sound and Vibration 2005; 294(3):547-561.
24. Wan Z, Cao H, Zi Y, He W, He Z. An improved time-varying mesh stiffness algorithm and dynamic modeling of gear-shaft system with tooth root crack. Engineering Failure Analysis 2014; 42: 157–177.
25. R Ma, Y S Chen. Research on the dynamic mechanism of the gear system with localized crack and spalling failure. Engineering Failure Analysis 2012; 26:12-20.
26. McFadden P D, Smith J D. Model for the Vibration Produced by a Single Point Defect in a Rolling Element Bearing. Journal of Sound and Vibration 1984, 96(1):69-82.
27. McFadden P D, Smith J D. The Vibration Produced by Multiple Point Defect in a Rolling Element Bearing. Journal of Sound and Vibration 1985, 98(2):263-273.
28. Tandon N, Choudhury A. An Analytical Model for the Prediction of the Vibration Response of Rolling Element Bearings Due to Localized Defect. Journal of Sound and Vibration 1997, 205(3):275-292.
29. D Ho, R B Randall. Optimization of bearing diagnostic techniques using simulated and actual bearing fault signals. Mechanical Systems and Signal Processing 2000, 14(5):763-788.
30. M.S. Patil et al. A theoretical model to predict the effect of localized defect on vibrations associated with ball bearing. International Journal of Mechanical Sciences, 2010, 52(9):1193-1201.
31. Sawalhi N, Randall R B. Simulating gear and bearing interactions in the presence of faults. Mechanical Systems and Signal Processing 2008; 22(8):1924-1951.
32. El-Thalji I, Jantunen E. A summary of fault modelling and predictive health monitoring of rolling element bearings. Mechanical Systems and Signal Processing 2015; 60-61:252-272.
33. Mohammed O D, Rantatalo M. Dynamic response and time-frequency analysis for gear tooth crack detection. Mechanical Systems and Signal Processing 2016; 66-67:612–624.

34. Park S, Kim S, Choi J H. Gear fault diagnosis using transmission error and ensemble empirical mode decomposition. Mechanical Systems and Signal Processing 2018; 108:262-275.

35. SX Jia, lan Howard. Comparison of localized spalling and crack damage from dynamic modeling of spur gear vibrations. Mechanical Systems and Signal Processing 2006; 20:332-349.

36. Saxena A, Parey A, Chouksey M. Effect of shaft misalignment and friction force on time varying mesh stiffness of spur gear pair. Engineering Failure Analysis 2015; 49: 79–91.

37. Sainsot P, Velex P, Duverger O. Contribution of Gear Body to Tooth Deflections-A New Bidimensional Analytical Formula. Journal of Mechanical Design 2004; 126:748-752.

38. Tian XH. Dynamic simulation for system response of gearbox including localized gear faults. Master's thesis, University of Alberta; 2004.

39. Palmgren A. Ball and Roller Bearing Engineering.3rd edn. Philadelphia: Burbank; 1959: 49-51.